Physical Properties of 3D Interconnected Graphite Networks - Aerographite

Karl Schulte
TECHNISCHEN UNIVERSITAET

10/30/2015
Final Report

DISTRIBUTION A: Distribution approved for public release.

REPORT DOCUMENTATION PAGE

1. REPORT DATE *(DD-MM-YYYY)*	2. REPORT TYPE		3. DATES COVERED *(From - To)*

4. TITLE AND SUBTITLE

5a. CONTRACT NUMBER

5b. GRANT NUMBER

5c. PROGRAM ELEMENT NUMBER

6. AUTHOR(S)

5d. PROJECT NUMBER

5e. TASK NUMBER

5f. WORK UNIT NUMBER

7. PERFORMING ORGANIZATION NAME(S) AND ADDRESS(ES)

8. PERFORMING ORGANIZATION REPORT NUMBER

9. SPONSORING/MONITORING AGENCY NAME(S) AND ADDRESS(ES)

10. SPONSOR/MONITOR'S ACRONYM(S)

11. SPONSOR/MONITOR'S REPORT NUMBER(S)

12. DISTRIBUTION/AVAILABILITY STATEMENT

13. SUPPLEMENTARY NOTES

14. ABSTRACT

15. SUBJECT TERMS

Aerographite, carbon nanostructures

16. SECURITY CLASSIFICATION OF:			17. LIMITATION OF ABSTRACT	18. NUMBER OF PAGES	19a. NAME OF RESPONSIBLE PERSON
a. REPORT	b. ABSTRACT	c. THIS PAGE			
					19b. TELEPHONE NUMBER *(Include area code)*

Performance Report:

Physical properties of 3d-interconnected graphite networks: Aerographite

Grant Number: FA8655-13-1-3058

Principal investigator: Prof. Dr.-Ing. Karl Schulte

Institute of Polymers & Composites

Hamburg University of Technology (TUHH)

Denickestr. 15

21073 Hamburg

Germany

Period of performance: May 2013 – March 2014

Summary

Aerographite is a novel carbon based cellular material consisting of a three dimensionally interconnected graphite structure. Aerographite is synthesized in a two step process: first, ZnO is manufactured, in a flame spray process forming a solid 3-D scaffold as template, followed by a CVD process in which the ZnO is covered by thin layers of graphite, while the ZnO template disappears. It exhibits excellent specific mechanical properties and a high electrical conductivity. The electrical properties are investigated within the scope of this project since they have not been studied in detail yet. The results of about the first year of this project are displayed in this performance report. The aim of this investigation is a description of electrical properties subject to different existing structural variants of Aerographite that vary in morphology and density.

The DC electrical resistance is measured as a function of compression of the Aerographite's structure. The samples show a high conductivity (about 2 S/m) and a piezoresistive behavior. The sensitivity is decreasing with the sample density. In cyclic loading and relaxation tests a time dependent behavior of the electrical resistance could be observed.

The dielectric properties are studied using AC impedance spectroscopy. A low capacitance can be measured that refers to good shielding properties of the material. Results are also obtained for different compression states. Similar to the DC-resistance a change in capacitance with compression can be observed here, too.

Furthermore electrochemical experiments are carried out. Aerographite is immerged in potassium chloride solution and the capacitance against a counter electrode is measured.

In order to correlate the results to the material's morphology a few first optical investigations using SEM (Scanning Electron Microscopy) and Raman spectroscopy are performed. In the last chapter further experiments needed are described.

Table of contents

List of Figures

1 Introduction

1.1 Aim of project

In a collaborative research between Hamburg University of Technology (TUHH) and the University of Kiel (CAU) we developed a novel approach to synthesize a light-weight 3-D structured graphitic scaffold, the so called Aerographite, in which the graphitic ligaments are directly interconnected by covalent bonds. This rare structural feature as a porous nanocarbon assembly is proposed to be the reason for the excellent specific mechanical and electrical properties.

Within the scope of this project we concentrate on the investigation of the electrical properties of this novel material which have not been studied in detail to date. Mechanical and other physical properties rather than electrical are to be investigated in separate German and European projects.

Due to the three dimensionally interlinked open porous structure with high surface area an excellent electrical DC conductivity and high capacity with AC current is expected. The aim of this project is to understand the electrical properties in context of the various adjustable inner structures of Aerographite and to find a correlation between them and the Aerographite's inner morphology.

1.2 Introduction of Aerographite

Aerographite is a novel carbon based nanomaterial formed to a 3-D network of directly interconnected thin-walled graphite layers with an ultralow density of some 200 µg/cm³ [1]. Its unique morphology causes a high absorption of electromagnetic radiation, high electrical conductivity and mechanical robustness which opens fields in application such as an electrode material in batteries and supercapacitors or as a filler for reinforcement of polymers.

Aerographite is fabricated in a newly developed two-step synthesis in which first a ZnO scaffold is produced in a flame spraying process [2], followed by a CVD process in which networks of tetrapod-like ZnO scaffolds are used as a template material. In the CVD process the ZnO scaffold is covered with graphitic layers, while the ZnO disappears. The formerly existing sintering bridges between the ZnO tetrapods are the reason for the resulting continuous, not interrupted and covalently bonded graphite network. In Figure 1.1 an SEM image of the ZnO template morphology is shown.
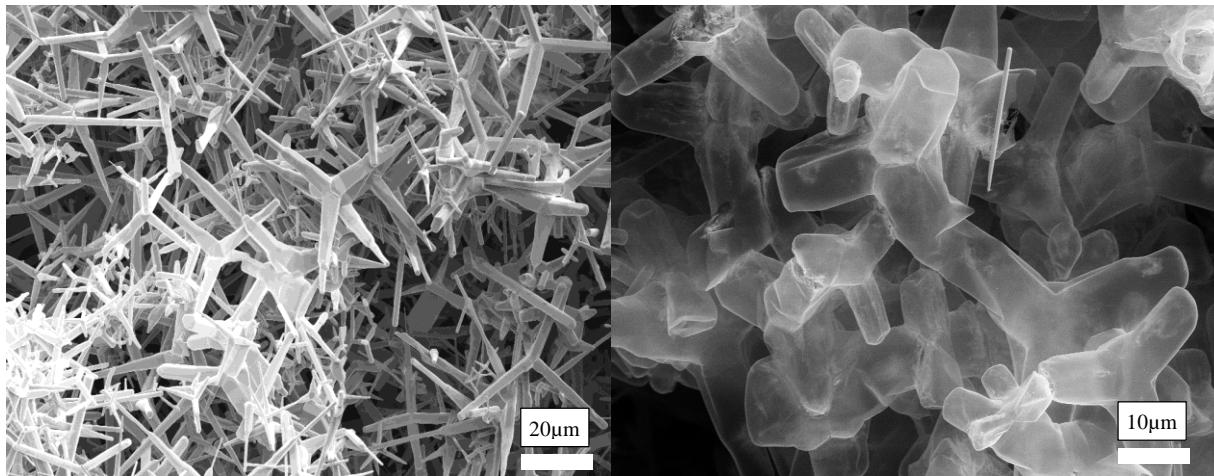
Figure 1.1: SEM image of ZnO Template (left) and Aerographite, only the graphite coverage remains

For production of Aerographite in the CVD process ZnO templates are placed in the maximum temperature zone of a two zone split tube furnace. At a constant temperature profile of 200° C in the injection zone and 760° C in main zone, a carbon precursor (toluene) is injected with a specific flow rate by a syringe pump. The toluene evaporates when entering into the furnace and forms graphitic layers on the ZnO scaffold. In a subsequent pure hydrogen treatment without injection the ZnO is reduced and precipitated to the exhaust system. The achieved Aerographite structure depends on the template surface area and time dependent variations of gas flow and toluene injection rates or temperatures. By controlling these CVD parameters, the Aerographite network can be tailored in morphology, wall thickness and also carbon species.

Three main structural variations of Aerographite can be produced:

a) The "closed-shell Aerographite" consists of thin-walled highly graphitic and 3-D-interconnected tubes with a wall thickness of about 10 nm and a tube diameter of 1-10 μm [1].

b) The "hollow-framework Aerographite" is a second hierarchical-level by formation of a network of carbon bands on top of former template surfaces. The porous wall structure results in an   ultra-low   density.

c) The "filled Aerographite" is the heaviest structure variant and consists of closed walls that are filled by what we suppose to be globular or lamellar graphitic carbon.

These manifold structural variants of Aerographite are supposed to have a direct influence on the electrical material properties. This relation is investigated within the course of this project. Therefore samples with different toluene injection rates were produced to regulate the sample density. Other parameters such as hydrogen gas flow rate and temperature were kept constant

over the different runs. In Figure 1.2 and Figure 1.3 the results from the synthesis runs are shown. The sample density is displayed as a function of the absolute toluene injection rate per time in Figure 1.2. The sample density is increasing with the injection rate.

In Figure 1.3 the density is displayed against the injection rate per time and also per mass of ZnO templates. Here, no direct correlation can be observed. Even for high injection rates only a medium density is obtained if the ZnO mass is low.
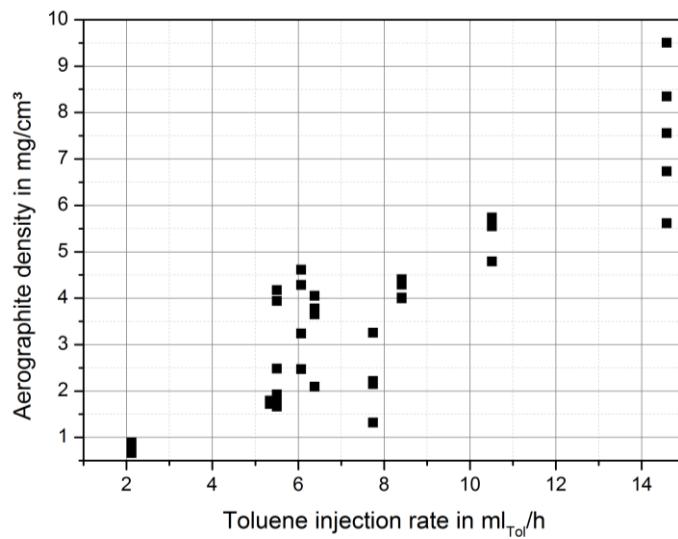
Figure 1.2: Influence of toluene injection rate per time on Aerographite density
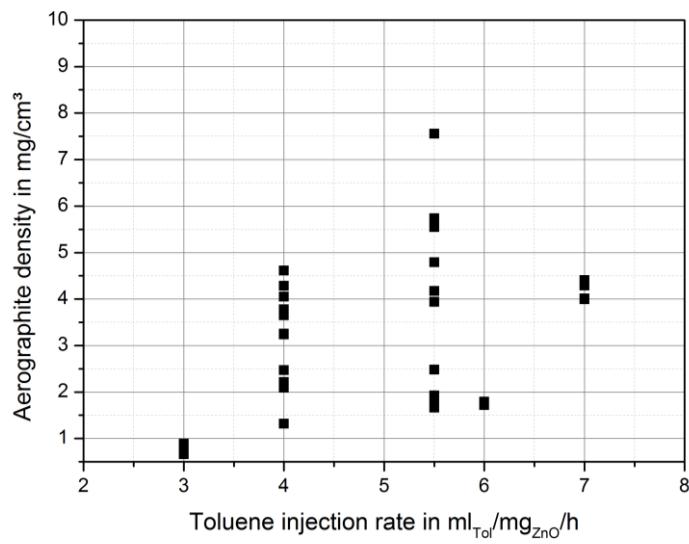
Figure 1.3: Influence of toluene injection rate per time and per mass of ZnO on Aerographite density

2   Methods and procedures

2.1 DC measurements under compression load

DC electrical conductivity measurements were performed for the different structure variants of Aerographite using a Keithley SourceMeter 2602 in a four-wire-configuration. The material was electrically contacted by pressing two plate-shaped electrodes of which one is translationally movable against its surfaces. To estimate the material's potential as a sensor material the electrical conductivity is varied by compressing and densifying the Aerographite samples between these electrodes while the resistance parallel to the compression direction is measured in situ. The DC resistance is then recorded as a function of displacement in compression. The experimental setup is shown in Figure 2.1.

The compressive force is quantified with a micro scales that measures the sample weight during compression. The compressive force is as well plotted as a function of displacement in compression and correlated to the resistance change curves.
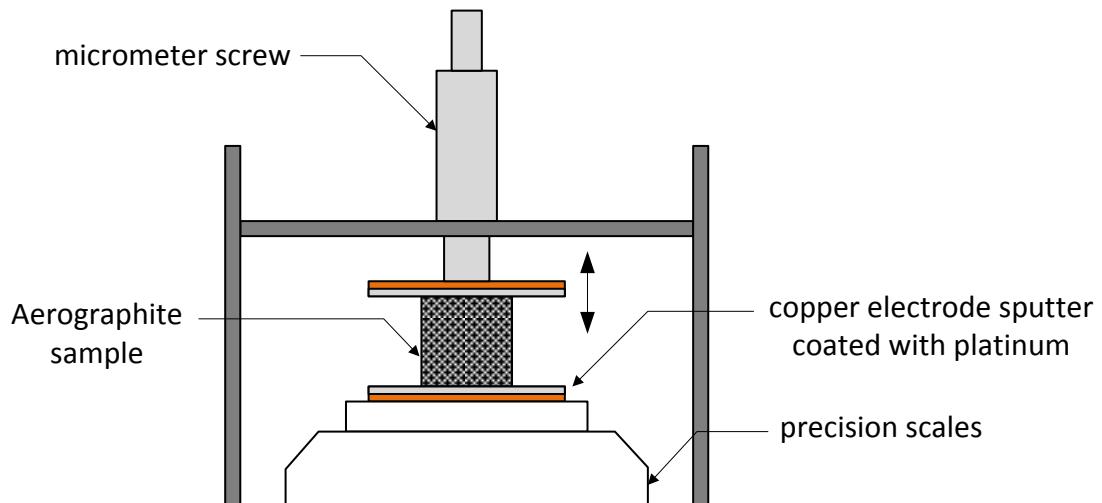
Figure 2.1: Experimental setup for DC electrical measurements

The electrode material was selected by recording R-I-curves for different electrode materials (Figure 2.2). To ensure that an ohmic contact is obtained the curve must be linear and no resistance drop should be observed with increasing current.
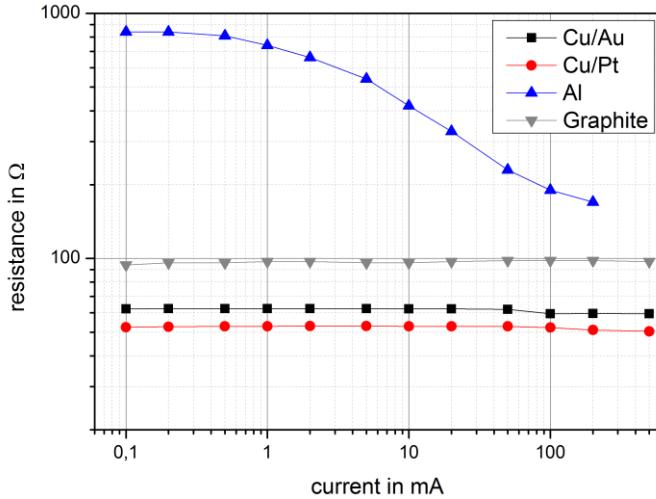
Figure 2.2: Measured resistance against current for different electrode materials

Copper electrodes sputter coated with platinum were selected as they show a linear resistance behavior versus the impressed current and the lowest absolute value for the resistance. The impressed current for the DC measurements was then set to 1mA.

2.2 Determination of sample density

To determine both the electrical conductivity and the stresses and strains geometrical sample data are needed. Aerographite is produced in volumes of 1cm³ and 2 cm³ of cylindric shape but as these structures tend to preferably collapse in the vertical center and become waisted the volume was measured using light microscopy. The sample height and width was measured in two different directions and the volume calculated.

2.3 AC measurements

AC electrical measurements were performed using an HP 4284a Impedance Analyzer and a four-wire-configuration. Impedance curves and capacitance as a function of AC current frequency were metered for three different compression states. The experimental setup was changed compared to the DC measurements by using a circular upper electrode that does not exceed the sample dimensions to avoid parasitic capacitances. As for the DC measurements the impressed current was set to 1mA. The current frequency is varied in a range from 20 Hz to 1 MHz.

2.4 Cyclic voltammetry

Electrochemical investigations were made performing cyclic voltammetry. In a cyclic voltammetry experiment the working electrode potential is ramped linearly versus time. The experiments were carried out using a potentiostat in a three-electrode-arrangement. The experimental setup is shown in Figure 2.3.

The Aerographite sample was connected to the working electrode and measured against a silver chloride reference electrode. As an electrolyte potassium chloride solution was used. The voltage was applied in a range between -1 and 1mV with different scan rates.
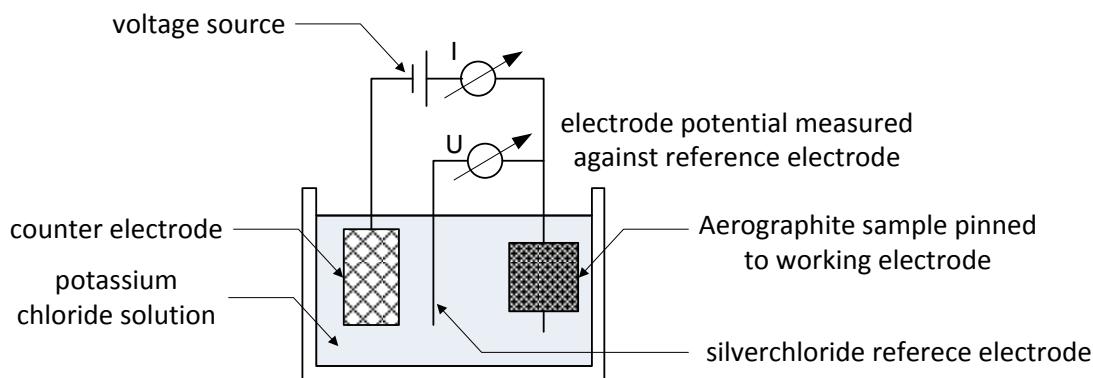
Figure 2.3: Experimental setup for cyclic voltammetry experiments

2.5 Raman Spectroscopy

Exemplary Raman experiments were carried out in order to give supporting information for the interpretation of the electrical data. Raman spectroscopy relies on inelastic scattering of monochromatic light, which in this case is a red laser. The laser light interacts with molecular vibrations, phonons or other excitations in the system, resulting in the energy of the laser photons being shifted up or down. As a correlation with this shift in energy Raman spectroscopy can for example deliver quantitative values for the evolving anisotropy if the open porous networks are unidirectionally deformed. By comparing these data with the electrical measurement data one can get a detailed description of the influence of the orientation of inner graphitic planes towards global material behavior.

Raman measurements were first conducted for the undeformed Aerographite. Detailed investigations for different compression states will be carried out later during this project.

3 Results and discussion

3.1 DC measurements under compression

In the following section the results of the DC electrical measurements are displayed. To connect the Aerographite to the measurement device the upper electrode was moved towards the sample surface until a resistance in the range of $M\Omega$ could be detected. In order to form comparable starting conditions the upper electrode was then moved a distance of 0,5mm closer. This point is defined as the initial position.
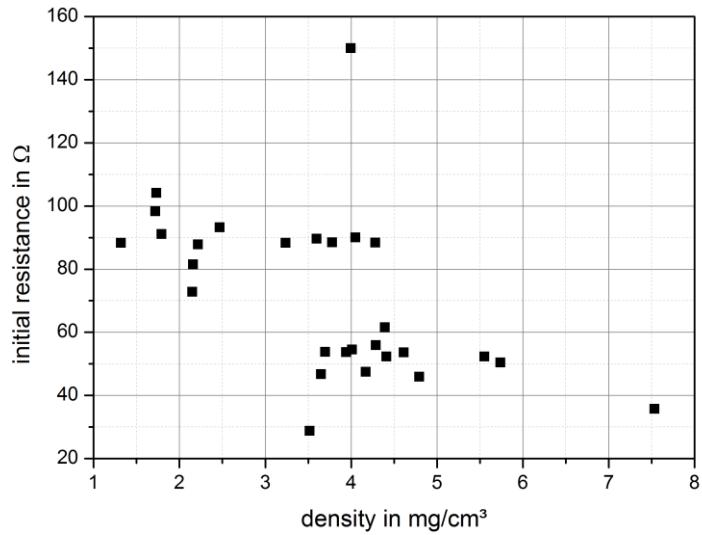
Figure 3.1: DC-resistance in the initial position as a function of density

In Figure 3.1 the initial values for the DC-resistance are shown for different samples as a function of density. A slight trend to a declining resistance with decreasing density can be observed which is probably due to the larger contact area of denser specimens.

3.1.1 Resistance and conductivity change curves under compression load

The samples were compressed displacement controlled up to a distance of one millimeter which, depending on the exact sample height, corresponds to a strain of about 10 to 15 percent.

The electrical resistance versus compression is shown in Figure 3.2 for three samples originating from three different synthesis runs with varying parameters, denoted as c95 (density: 3,5 mg/cm²), cg2 (2,2 mg/cm²) , cgc7 (5,77 mg/cm²). The corresponding SEM-images are shown in Figure 3.3. The synthesis c95 reveals a structure that seems to be hollow but with closed stiff tetrapods. In the middle picture the lightest version of the three samples is shown. The structure is also hollow and closed but apparently thinner-walled and wrinkled. The structure of the synthesis cgc7 is a filled Aerographite variant.
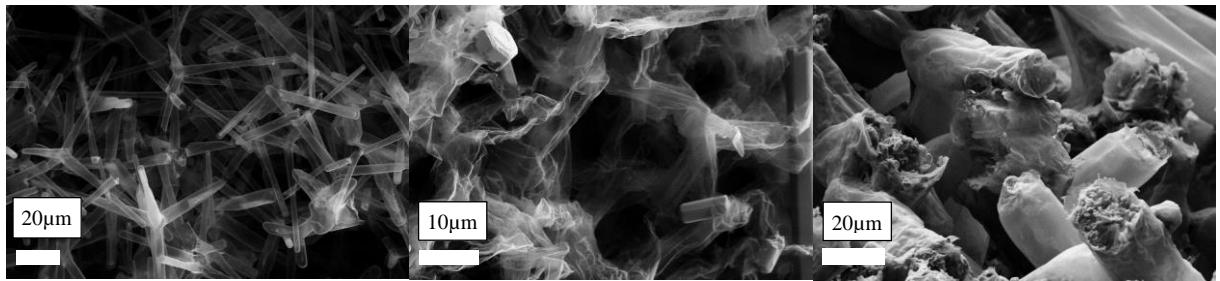
Figure 3.2: SEM-image of different Aerographite samples (from left to right: c95, cg2, cgc7)
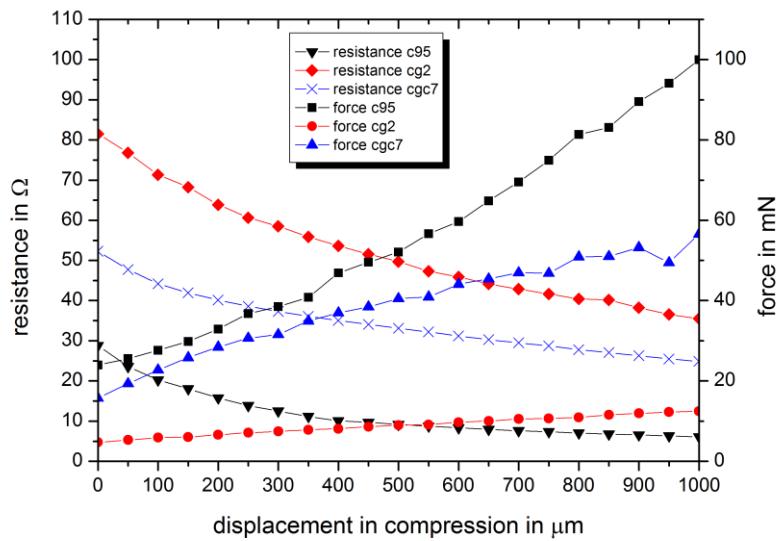
Figure 3.3: Resistance and force as a function of displacement in compression

It can be seen that for all samples the resistance is decreasing with increasing displacement in compression. The curves progressions show a steeper decrease at the beginning and flatten while approaching a constant value. The steeper decrease in resistance at the beginning can partly be explained with the increasing contact area between the tetrapod-like graphitic tubes and the electrodes. As the curve is flattening the influence of the contact resistance is reduced

but the further drop in resistance is mainly caused by the increasing number of inner contacts of Aerographite's tetrapod arms. At a certain level of compression a further compacting of the structure has only very little influence on the resistance behavior. The maximum contact area between the tetrapods is already reached. In Figure 3.4 a schematic of the explanation depicted above is visualized.
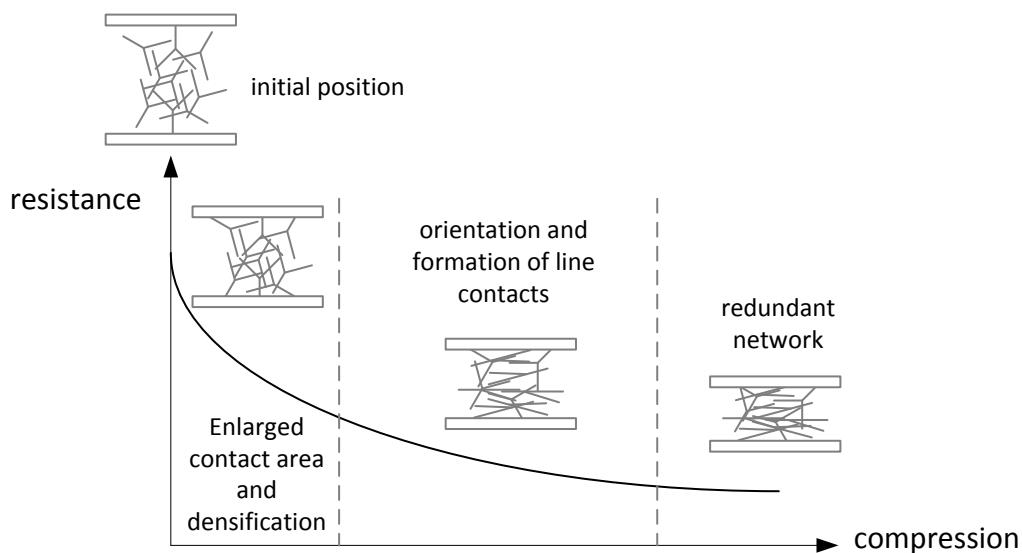
Figure 3.4: Schematic of the development of resistance curve progression

The absolute value for the difference between initial and final resistance against the compression distance is decreasing with increasing sample density. This observation can as well be explained with the fact that for a higher sample density the third state shown in Figure 3.4 is beginning earlier and at less compaction.

The compressive force shows an antiproportional behavior compared to the resistance. For all samples an increase in force is detected. For the most lightweight of the three samples shown, cg2, this increase is small and almost linear. The two denser samples c95 and cgc7 exhibit a similar behavior up to a displacement in compression of about 0,4mm, then the sample cgc7 follows a declining curve whereas the sample c95 shows a progressive behavior. The little increase in force of the sample cg2 can be explained with its capability to dissipate energy while being compacted. For the medium light sample this phenomenon is less pronounced, which results in a steeper force increase. The appearance of a declining curve for the heaviest sample of Aerographite is expected to be due to the stiffness of the tetrapods which do not allow a constant compression rather than a sudden buckling of the structure. That causes the observed flattening of the curve.

In Figure 3.5 the conductivity and the stress are plotted against strain. The height of stress seems to be crucial for the increase of conductivity.
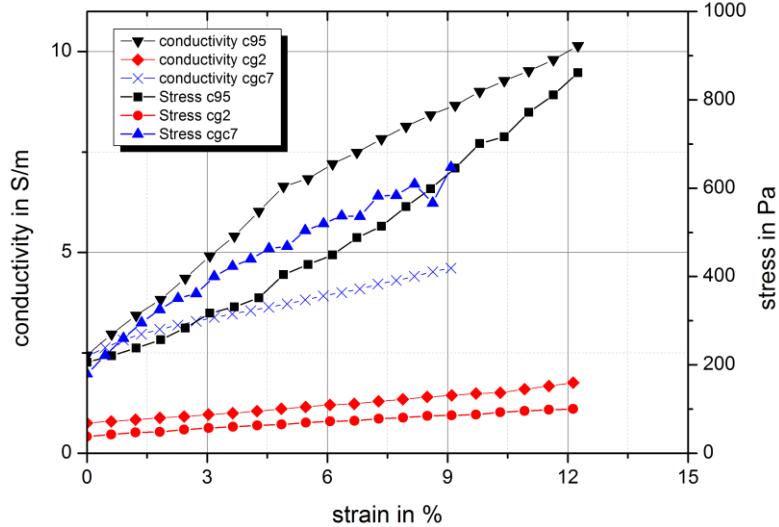
Figure 3.5: Conductivity and stress as a function of strain

From the conductivity values the sensitivity (gauge factor) can be derived which is defined as the ratio of the resistivity change divided by the elastic strain. As indicated in Figure 3.5 the strain is approximately linear over the whole displacement. Figure 3.6 shows the relation between the gauge factor and the density of the Aerographite.
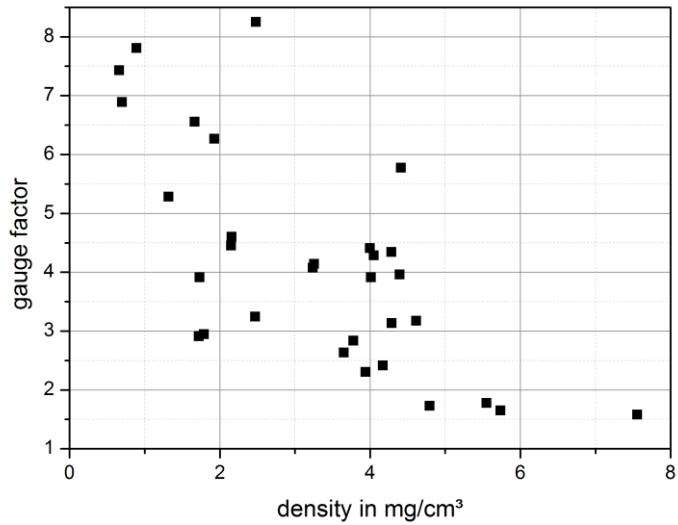
Figure 3.6: Development of gauge factors under compression load for different sample densities

The sensitivity shows a strong dependence on the sample density. As can be seen the gauge factor is decreasing from values between seven and eight for lightweight Aerographite with a

density below 1mg/cm³ to values between one and two for the heavier structure variants with a density of above 5 mg/cm³. In Figure 3.7 the gauge factor is displayed as a function of the relative compressive stress change. As expected, a correlation exists here as well. The gauge factor is decreasing with increasing stress change. The scattering is even less than for the correlation with the sample density so that the density may not be the main influencing factor for the piezoresistive behavior. Further investigations will be carried out in the future to examine this assumption.
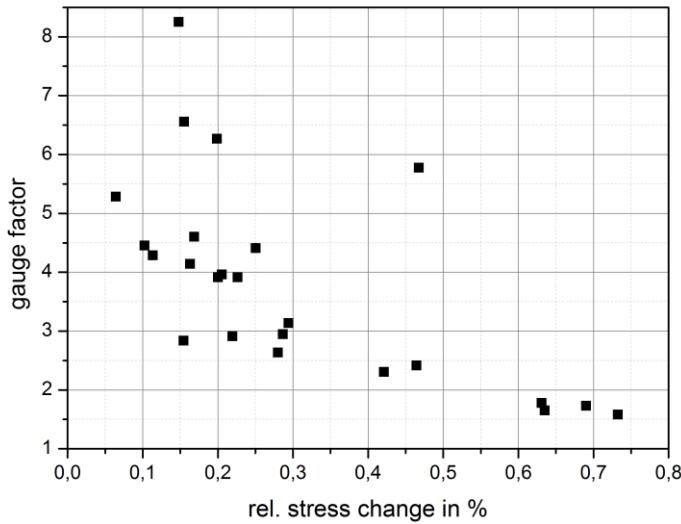
Figure 3.7: Dependency of gauge factors on relative stress strange under compressive load

3.1.2 Resistance and conductivity change for loading and unloading

For several samples the resistance behavior was not only tested for compression load but also for loading and unloading. The samples were compressed up to a displacement of 2mm, then fully unloaded and afterwards in a second cycle loaded again displacement controlled until a displacement of 2 mm was reached again and then finally unloaded. In Figure 3.8 the plot of resistance change as a function of displacement is shown. The sample shown originates from the synthesis cg9 and has a density of about 1,8 mg/cm³.

As for the experiments where only one compression cycle was detected the resistance is decreasing with further compression. When unloading the resistance is increasing again in a steeper curve progression than for loading. The initial resistance of about 90 Ω is already reached at a displacement of 1250 µm, for lower compression the resistance exceeds the initial value. From this observation can be concluded that the Aerographite remains to be permanently deformed.
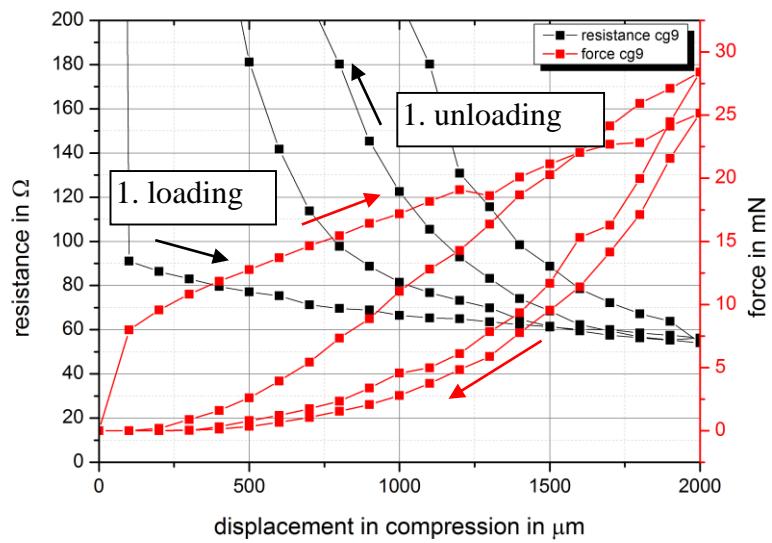
Figure 3.8: Resistance as a function of displacement in compression for two loading and unloading cycles.

For the second load cycle the resistance curve is again shifted to lower displacements. The initial value of resistance is already reached at about 800 µm displacement. Thus, the Aerographite seems to unfold itself again after removing the load. For the second unloading cycle the curve is shifted to the right to higher displacements in compression compared to the first unloading cycle, which means that the permanent deformation has become larger.

The force in the first load cycle is increasing almost linearly (to be precise slightly declining) but shows a progressive course when the sample is unloaded. This is again an evidence for a remaining deformation. In the second load cycle the curve is increasing progressively and much steeper than in the first load cycle. The final value of compressive force is with about 28mN higher than the value of 25mN reached in the first load cycle, so a cyclic solidification of the structure can be observed.

The cyclic loading and unloading has not been investigated up to date in detail for different structure variants. Especially samples synthesized with low injection rates were not tested. The sample cg9 has a relatively low density but was fabricated with high toluene injection rates from a low weight of ZnO template. As indicated in chapter 1.2 in Figure 1.3 the amount of ZnO is also crucial for the received density. The sample cg9 shows a similar behavior as the samples with a high density. It is to examine in the course of this project if for lightweight Aerographite fabricated with "light parameters" the results differ from what is shown in Figure 3.8.

3.1.3 Time dependent resistance behavior

In the cyclic loading and unloading experiments an "unfolding" of the Aerographite structure was observed, indicating a time dependent mechanical and accordingly time dependent electrical behavior. To further examine this fact relaxation tests were carried out. The sample was loaded beginning from an initial position in four steps whereat in every step the displacement in compression was increased by 500 µm and afterwards unloaded. The resistance and force were recorded as a function of time over 20 minutes per step as depicted in Figure 3.9 for a heavier structure variant with a density of about 4 mg/cm³.
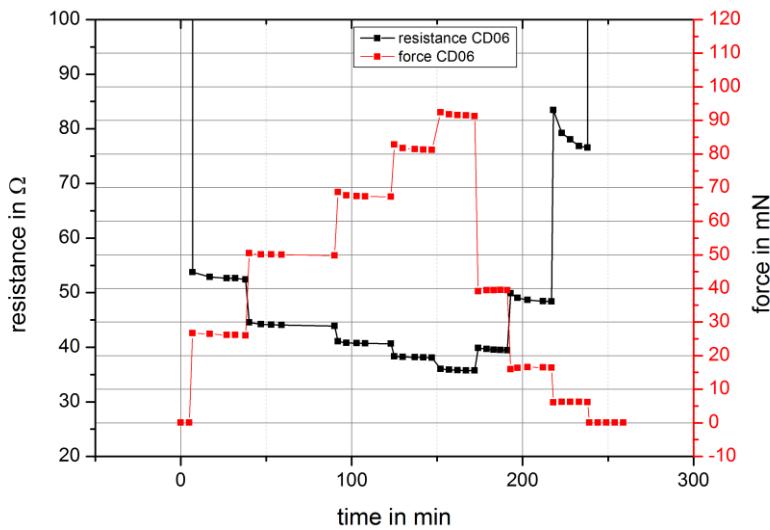
Figure 3.9: DC-resistance and compressive force as a function of time for four compression and unloading steps

During loading both the resistance and the force are decreasing with time. The decrease in force can be explained by a slow yielding and relaxation of the structure under compression load. The decrease in resistance is thus also expected to be due to the increasing amount of junctions that result from yielding. With every compression step the decrease in force becomes larger in absolute values but less in percentage. After the first compression step the decrease amounts about 2,5 %, after the last compression step it is only 1,1 % decrease. The denser the structure is compacted the less it can yield. The resistance curve is showing the same trend accordingly.

For unloading the resistance is increasing with every unloading step but still follows a declining curve progression against time. This could again be stated with the unfolding of the structure. Therefore, also the force shows the behavior to be seen in the diagram. This relaxation behavior was observed for different densities similarly.

3.2 AC measurements

In this section the results from AC electric measurements are presented. The investigations on impedance and capacitance followed the same procedure described in section 3.1. All the measurements were also carried out beginning from the defined initial position.

3.2.1 Impedance spectra

As for the DC measurements the samples were brought into the initial position and their impedance was recorded as a function of current frequency. The same was done for two further compression states at 500µm and 1500µm compression. The results for sample cg2 are displayed in Figure 3.10. This figure implies the impedance is almost independent of frequency and shows only small scattering for the least compressed position. The three compression states are clearly to be determined.
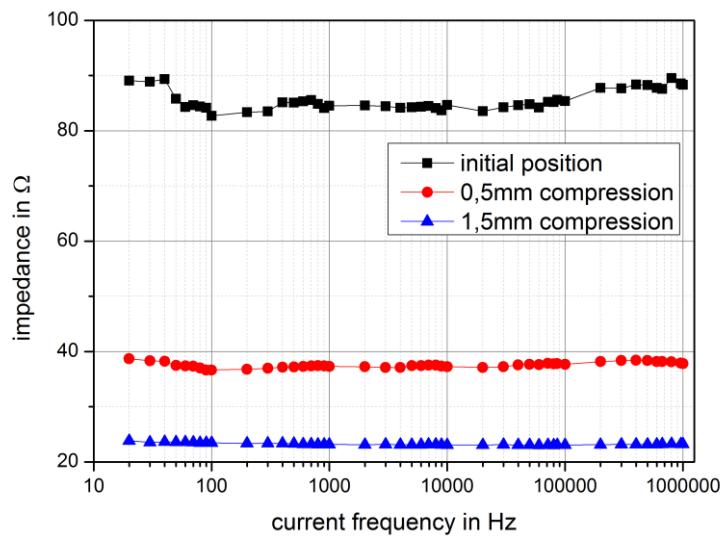
Figure 3.10: Impedance as a function of current frequency

Due to the open porous structure and high surface area the Aerographite structure is supposed to carry a lot of charge between facing surfaces. Therefore a capacitive behavior with AC current is expected. Since there exist, besides the facing surfaces, also a lot of connected conducting paths the structure can be simplified as a parallel circuit of capacitance and ohmic resistance, as shown in Figure 3.11. The impedance can be split into a real part, the ohmic resistance R, and an imaginary part, the reactance X. If the reactance is plotted as function of resistance this gives the so called Nyquist plot. The Nyquist plot for the impedance spectra above is visualized in Figure 3.12. In Figure 3.11 the theoretical Nyquist plot for an ideal parallel circuit of capacitance and resistance can be seen.
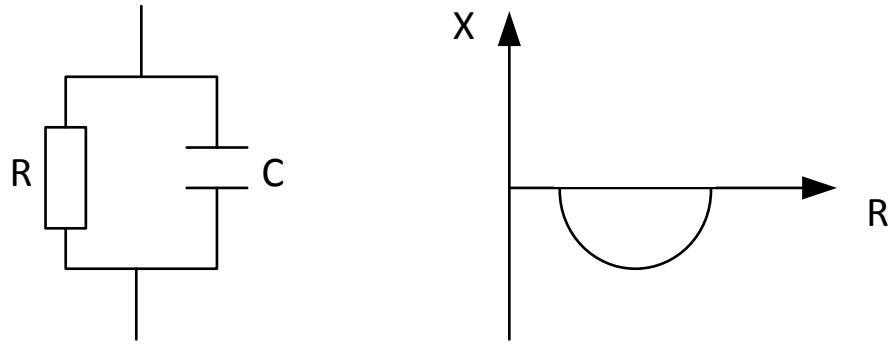
Figure 3.11: Parallel circuit of resistance and capacitor (left) and Nyquist plot of reactance against re-
sistance (right)
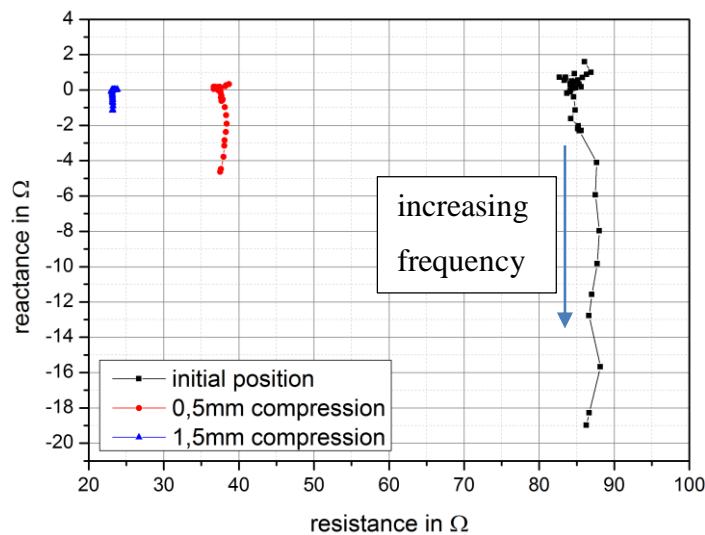
Figure 3.12: Nyquist plot of sample cg2 for three compression states

It can be concluded that the impedance is dominated by the real part, the ohmic resistance. The
reactance influence is only minor to the overall impedance. As for the theoretical curve the
reactance proceeds into the negative range but does not describe a whole semicircle. With every
compression step both the reactance and the resistance are decreasing. According to the equa-
tion

$$C = \varepsilon * \frac{A}{d}$$

the capacitance C of a plate capacitor is increasing the smaller the distance d between the two
conducting surfaces of the area A. The capacitive reactance is correlating in inverse proportion
with the capacitance according to the equation

$$X = -\frac{1}{2\pi f * C}$$

where f is the current frequency. This correlation is depicted in the Nyquist plot.

3.2.2 Capacitance curves

As for the impedance the capacitance was also measured as a function of current frequency. Again the samples where compacted in three steps. For the sample cg2 the dependency of the capacitance from the current frequency can be seen in Figure 3.13. Most conspicuous is that a stable value of capacitance is not reached before a current frequency of about $2 * 10^5$ Hz. In addition the capacitance lies in the order of 10^{-11} F which is very small.
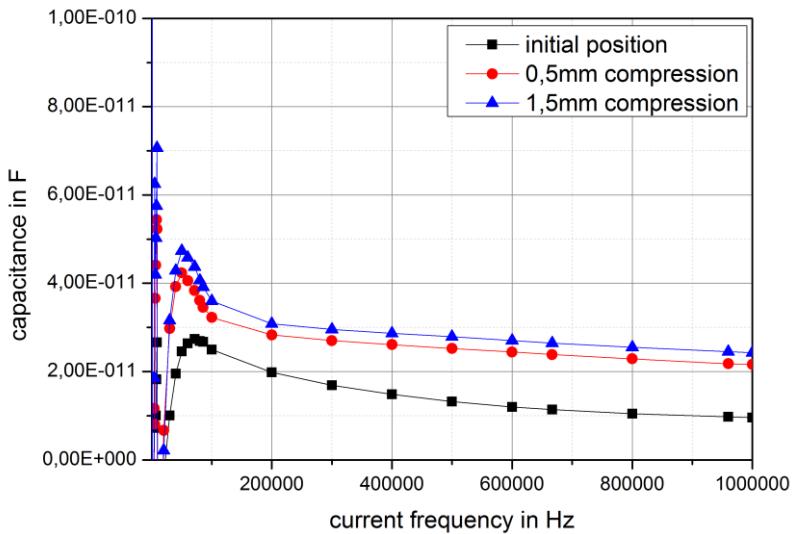
Figure 3.13: Capacitance as a function of frequency

For frequencies lower than $2 * 10^5$ Hz the values for capacitance are jumping in a wide range from negative to positive. One explanation could be the measurement frequency which at low frequency levels is also low and allows the "capacitor" to load and unload several times within one measurement cycle. The increase in capacitance for further compaction of the structure is also given in the plot.

Capacitance measurements were performed for all samples produced. In Figure 3.14 the measured capacitances are displayed against the sample density. A large scattering of the values can be observed and a correlation between capacitance and density can hardly be identified.
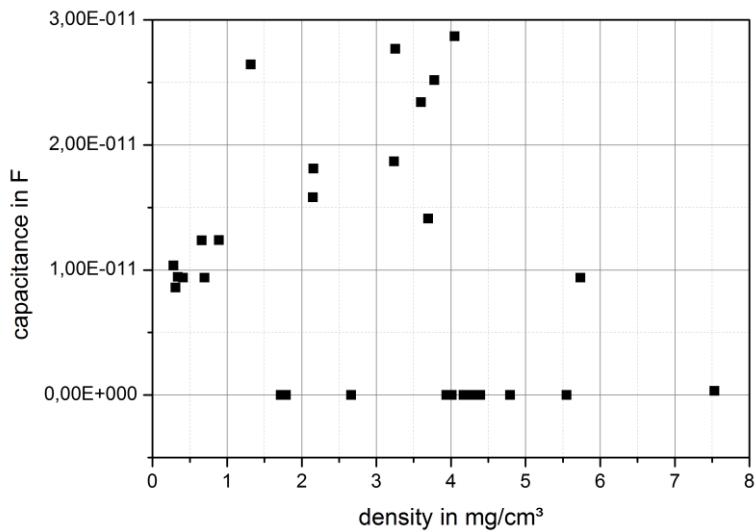
Figure 3.14: Distribution of capacitances versus different sample densities

A noticeable fact is that for some samples no capacitance could be measured. For these samples the value of the capacitance was set to zero in Figure 3.14. Although these samples are all of a different density they were all produced in selected processes which means that there were batches produced in which all the sampled did not exhibit any capacitance. In Figure 3.15 the distribution of capacitances is shown against the carbon precursor injection rate.
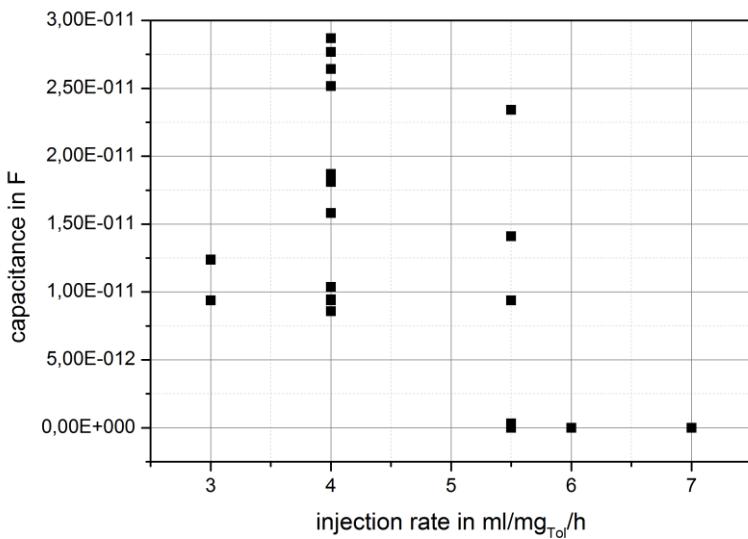
Figure 3.15: Capacitance as a function of carbon precursor injection rate

What can be observed is that for high injection rates (5,5ml/mg/h and more) the Aerographite does not exhibit a capacitance any more although the resulting density (which according to

Figure 1.3 is not only depending on the injection rate) is low and a hollow structure with lots of facing surfaces is expected. For the "high injection produced" Aerographite no SEM pictures had been taken yet. This is an important part of the further work plan.

Besides it could be observed that the same samples which did not exhibit a capacitance showed a declining force curve during compression. This is an indication that by varying the injection rate not only the density but especially the morphology. It seems that samples of the same density may nevertheless show different morphologies.

3.3 Cyclic voltammetry

In the following the results from electrochemical studies by cyclic voltammetry are presented. Cyclic voltammetry was performed first in absence of an electrolyte and later in potassium chloride solution.

3.3.1 Voltammetry without electrolyte

For the measurements without a liquid electrolyte the setup was modified from what is shown in Figure 2.3 insofar as the working electrode and the counter electrode were short-circuited by connecting them both to the Aerographite sample. The result for sample cg2 is given in Figure 3.16. The current density is increasing linearly with the voltage and is independent of the voltage scan rate (in the plot only one scan rate is shown). This indicates again that Aerographite just in air shows the behavior like an ohmic resistor. The small capacitance the material holds cannot be determined with this method.
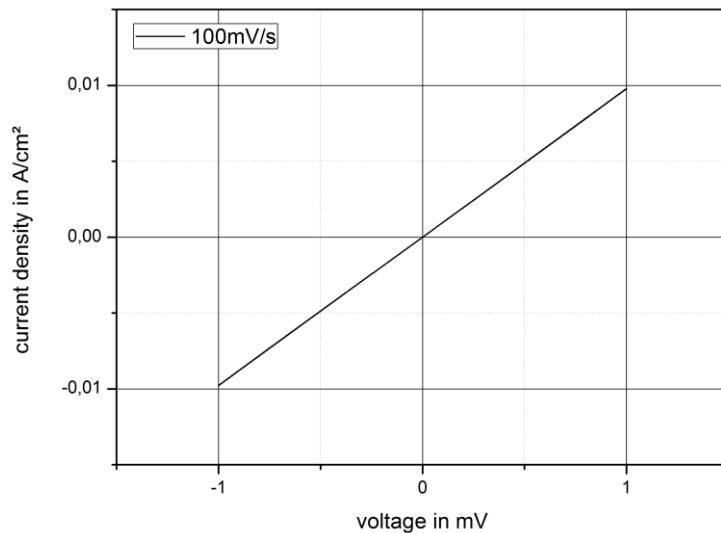

Figure 3.16: Current density as a function of voltage during cyclic voltammetry experiment

3.3.2 Voltammetry with electrolyte

In a second step potassium chloride solution was used as an electrolyte. Cyclic voltammetry experiments were performed for three different scan rates. In Figure 3.17 the results are displayed. For all scan rates a hysteresis loop can be observed. By increasing the voltage scan rate the loop becomes narrower. The specific capacitance per surface area correlates with the area enclosed by the hysteresis loop. Thus the specific capacitance is decreasing with the voltage scan rate. The specific capacitance can be calculated as the integral of current density.

For a scan rate of 100mV/s the specific capacitance is about 23F/cm².
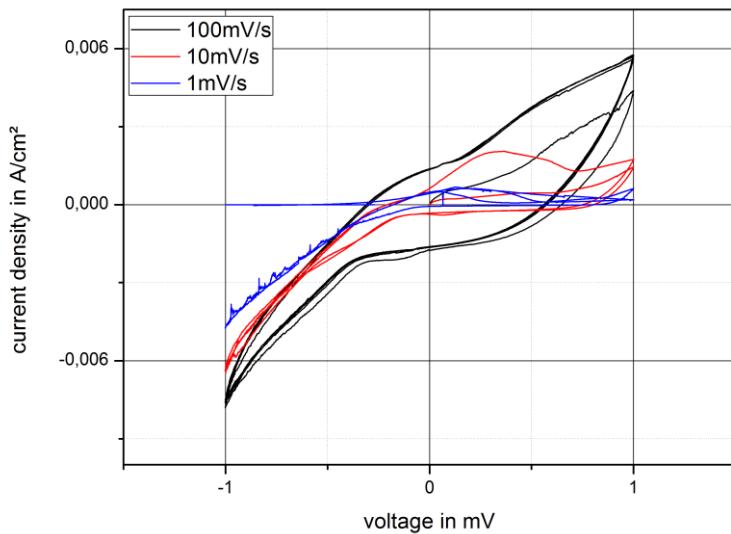
Figure 3.17: Current density as a function of voltage for different scan rates

The quality of the electrode can as well be estimated with the method of cyclic voltammetry. The ideal capacitor exhibits a hysteresis loop with a square geometry. The more the loops are similar with varying scan rates, the better the diffusion processes in the electrode work. For the scan rate of 1mV/s the limit seems to be reached because almost no current flow is possible any more. Cyclic voltammetry was not yet carried out comprehensively but is planned for future investigations.

3.4 Raman spectroscopy

Raman spectra were recorded for two material orientations. For both measurements the laser was focused directly on an arm of the tetrapod structure. In Figure 3.18 the resulting Raman spectra are displayed. Two pronounced peaks can be observed in both spectra, the D peak at about 1350 cm^{-1} and the G peak at about 1580 cm^{-1} which are typical for carbon based materials. In case of the D peak, a charge carrier has to be excited and inelastically scattered by a phonon,

then a second elastic scattering by a defect must occur to result in a recombination. Therefore for pristine graphene no D peak occurs. The Raman spectrum for the tested Aerographite lies in between the spectra of neat graphene and graphene oxide.

By determining the ratio of the corresponding intensities I_G/I_D an estimation about the graphite quality and graphitization can be made. For the sample shown in the plot this ratio has the value 0,88. For a ratio below 1 the D band is more pronounced than the G band which can lead to two conclusions. There is a regime of high defect density where D will increase as a higher defect density creates more elastic scattering or there is a regime with a lot of functional groups.
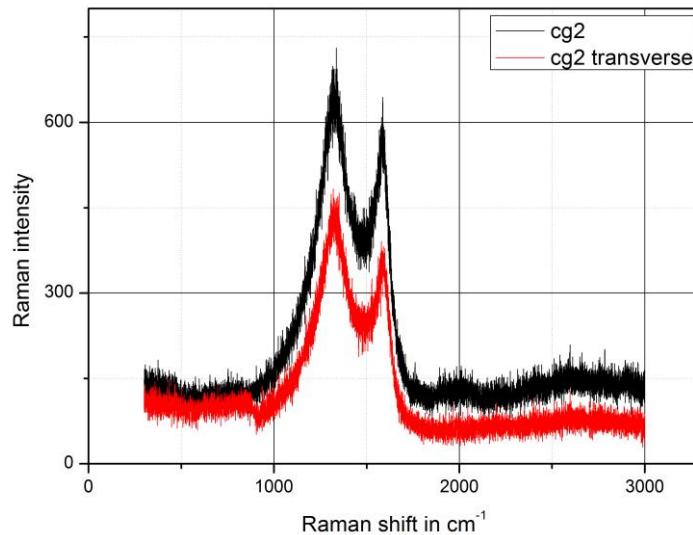
Figure 3.18: Raman spectrum for specimen cg2 in two orthogonal directions

The second overtone of the D peak, the 2D peak, cannot clearly be observed. It is maybe again suppressed by functional groups. The presence of functional groups will be further investigated using X-ray diffraction in the future.

The second spectrum taken in transverse direction exhibits the same peak position as in the orthogonal direction. Only the Raman intensity is minor than before. This could be due to either less material the laser was focused on and therefore less reflection or possibly a higher amount of remaining ZnO particles that give higher fluorescence effects.

Raman measurements will be conducted systematically for different structure variants in the future.

4 Conclusion

The aim of this project is to study and describe in detail the electrical properties of Aerographite and its correlation with its unique and tunable morphology. Samples of different density were produced in the CVD process. A first interrelation between the density and the morphology could be identified by taking SEM pictures. The lightweight structure variants exhibit a rather thin walled and electron microscopically transparent structure whereas the heavier variants show a higher contrast, which is an indication for a thicker walled structure.

In the DC resistance tests the cylindric Aerographite samples of 1cm² or 2cm² size show a low initial resistance between 50 and 100 Ω. The initial resistance is depending on the sample density in inverse proportion. Furthermore the samples exhibit a piezoresistive behavior as their resistance decreases with increasing displacement in compression. Their gauge factor can assume values from about 1,5 to 8 where the most lightweight structure has the highest gauge factor. This makes the material applicable as an ultra-lightweight sensor material when small strains appear and high sensitivity is required. Under cyclic loading the material shows a cyclic hardening. Under constant load a relaxation can be observed. In AC resistance measurements a low capacitance over a large range of frequencies could be observed. As a low capacitance leads also to a low permittivity these results display the ability of Aerographite for shielding radiation of different frequencies. No correlation could be observed for the distribution of capacitance over sample density. In cyclic voltammetry experiments in potassium chloride solution it could be shown that it is possible to wet respectively cover the Aerographite structure with the electrolyte. Furthermore a high capacitance per unit area could be measured. This is a first indication for qualifying the materials for applications like the use as electrodes in capacitors.

Aerographite shows great potential in different fields of applications. To better understand the correlation between morphology and electromechanical properties and in order to tailor it towards application more precisely further investigations, as described in the next chapter, will be carried out.

5 Further work plan

As already mentioned above further investigations need to be done within the scope of this project. These are:

Scanning Electron Microscopy

All the samples will comprehensively be investigated using Scanning Electron Microscopy in order to characterize their morphology. Furthermore, the ZnO-Templates are also analyzed by SEM to compare the structure before and after synthesis and to correlate the physical properties also with the ZnO morphology.

DC measurements for loading and unloading

Additionally to the DC-resistance under compression the DC-resistance for unloading the samples will also be recorded. Information about the time dependent mechanical and electrical properties are expected to be achieved.

DC measurements in perpendicular direction

If possible the samples will be contacted perpendicular to the compression direction and the resistance change will be recorded, too. It should be possible to specify a factor of unisotropy.

Electrochemical measurements

All samples will be investigated by cyclic voltammetry in an electrolyte. Impedance spectra in presence of an electrolyte will be recorded. The active surface of the samples and the capacitance per unit area will be determined. This examination is the last examination step for a single sample because the structure is finally coated by an electrolyte.

Investigation of larger range of density

Most of the samples investigated are of medium density. In further synthesis steps samples with ultralow density ($<1mg/cm^2$) and with high density ($>5mg/cm^2$) will be produced. Those with

a high density which will probably exhibit a filled structure. All the examinations reported here will also be carried out for the new samples.

Optical investigations

All samples will be characterized by EDX to determine the element composition and purity of the samples. X-Ray diffraction will be used to study the number of graphite layers and the spacing in between. Raman measurements will be performed comprehensively to get information about the graphite quality and isotropy of the material.

An overview of the further studies planned is given in Table 5.1.

Table 5.1: Workplan for the next half year

	April	May	June	July	August	September
SEM, EDX	■	■	■	■	■	■
Synthesis of other densities			■	■	■	
DC measurements load unload	■		■	■	■	
Perpendicular direction		■	■			
Electrochemical measurements					■	■
XRD, Raman		■	■	■		

References

[1]   M. Mecklenburg, A. Schuchardt, Y.K. Mishra, S. Kaps, R. Adelung, A. Lotnyk, L. Kienle, K. Schulte *Aerographite: Ultra lightweight flexible nanowall carbon microtube-material with outstanding mechanical performance.* Advanced Materials, 24(26), 2012. DOI: 10.1002/adma.201200491 (2012)

[2]   Y. K. Mishra ,* S. Kaps , A. Schuchardt , I. Paulowicz , X. Jin , D. Gedamu , S. Freitag , M. Claus , S. Wille , A. Kovalev , S. N. Gorb, R. Adelung: *Fabrication of Macroscopically Flexible and Highly Porous 3D Semiconductor Networks from Interpenetrating Nanostructures by a Simple Flame Transport Approach.* Part. & Part. Syst. Charact. 30(9) (2013) 775-783

List of abbreviations

AC   alternate current

C95, CG2   denotation for synthesis processes

CVD   Chemical vapour deposition

DC   direct current

EDX   energy dispersive X-ray spectroscopy

SEM   Scanning electron microscopy

XRD   X-ray diffractometry

ZnO   zinc oxide

List of Units

cm   centimeter

cm²   square centimeter

cm³   cubic centimeter

F   Farad

h   hour

Hz   Hertz

mA   milliampere

mg   milligram

ml   milliliter

mm   millimeter

mN   millinewton

MΩ   megohm

mV   millivolt

μg   microgram

μm   micrometer

Ω   Ohm

Pa   Pascal

List of symbols

A   area

C   capacitance

d   distance between capacitor electrodes

ε   permittivity

f   fequency

I   current

I_D intensity of D band

I_G intensity of G band

R   resistance

X   reactance